PSIG 2103

Performance of CPM Based Leak-Detection Algorithms in the Presence of Slack

Hamed Ghasvari Jahromi [1], Fatemeh Ekram [1], Waqar Ali [1], Michael Roxas [1], Satya Mokamati [1]

[1] Vanmok Leak Detection Technologies Inc.

This paper was prepared for presentation at the PSIG Annual Meeting to be held virtually on 3 May – 7 May 2021.

ABSTRACT

Leaks may occur at any time and location in a liquid transmission pipeline. One of the significant complexities in the leak detection process arises when the leak happens in a pipeline in the presence of phase change. A set of experiments are conducted on a 374-meter (1227-ft) pipe to examine the performance of CPM-based Leak-Detection algorithms. Different intensities of slack from the bubbly flow to the complete cavitating zone are managed to be present before performing various leak tests in terms of size and location. Flow and pressure values are measured at different locations along the length of the pipeline and used as the initial and boundary conditions or constraint points and fed to the algorithms. Two CPM-based leak detection algorithms are considered. The first algorithm performs the leak detection based on a CPM model, which does not model the hydraulics involving phase change. The second algorithm takes advantage of a CPM solver with a precise model to take phase change (cavitation) and the presence of vaporous phase (slack) into account. The ability and quality of these leak detection algorithms are examined against the experiments. The results show the importance of the phase change modelling ability of the CPM to avoid false positives and detect the leaks of different types, which would have otherwise been masked under operating conditions that involve phase change.

INTRODUCTION AND BACKGROUND

In this paper, CPM-based leak detection algorithms are classified and critically examined to study their influence on the performance of the leak detection systems. By conducting experiments on a flow-loop, we generated the data to compare two classes of these algorithms. The Leak detection using one class of these algorithms is reliable and keeps a robust performance in scenarios during simultaneous leak and slack. In contrast, the other class consistently performs reliably and robustly.

In this paper we are considering model algorithms to be the basis of the CPMs to study their influence on the detectability of leaks under slack flow conditions. Hence, we consider only one significant difference between the two LDS models in the CPM, which provides “calculated data” for the leak detection process (see Figure 4). The two compared algorithms differ in their formulation leading to two types of calculated data passed to the alarm module shown in Figure 4. We want to know if the CPM basis can be the root cause of any reliability issues, including missing any leak or generating false alarms. Hence, we apply the operating condition of the test cases to see if the CPM model makes any difference.

APPROACH

We categorize the models and their algorithms for this paper into two general categories. The ones whose models and their formulation are not primarily to deal with or capture interfacial mass transfer; Three well-known models of such kind are Discrete Vapor Cavity Model (DVCM), Discrete Gas Cavity Model (DGCM), and Generalized Interface Vapor Cavity Model (GIVCM). Equations (1) and (2) are continuity and momentum equations, respectively, without an explicit term for interfacial mass transfer during phase change.

$$\frac{1}{c_0^2}\frac{\partial P}{\partial t}+\frac{\rho_l}{\pi r_0^2}\frac{\partial Q}{\partial x}=0 \quad (1)$$

$$\frac{\rho_l}{\pi r_0^2}\frac{\partial Q}{\partial t}+\frac{\partial P}{\partial x}+F_0(Q)+\rho_l g\sin(\theta)=0 \quad (2)$$

DVCM assumed that the vapor cavities formed at any computing sections of the pipe if the pressure drops to the vapor pressure. DGCM is one of the variations of DVCM where a small quantity of gas is assumed to be present at computational nodes initially.

Each small volume of gas isothermally grows or collapses as the pressure changes according to the ideal gas equation. GIVCM includes complete sets of separate coupled governing equations to model column separation and correctly control the various phase interactions.

The four sets of equations describing GIVCM form seven governing equations presented in Equations 3-9, as discussed in [8].

- Water Hammer Equations:

$$\frac{\partial H}{\partial t}+V\frac{\partial H}{\partial x}-V\sin\theta+\frac{a^2}{g}\frac{\partial V}{\partial x}=0 \quad (3)$$

$$g\frac{\partial H}{\partial x}+\frac{\partial V}{\partial t}+V\frac{\partial V}{\partial x}+\frac{fV|V|}{2D}=0 \quad (4)$$

- Two-Phase Flow Equations for Distributed Vaporous Cavitation Region:

$$\frac{\partial \alpha_v}{\partial t}+V_m\frac{\partial \alpha_v}{\partial x}-\frac{\partial V_m}{\partial x}=0 \quad (5)$$

$$\frac{\partial V_m}{\partial t}+V_m\frac{\partial \alpha_v}{\partial x}+g\sin\theta+\frac{fV_m|V_m|}{2D}=0 \quad (6)$$

- Shock Equations for Condensation of Liquid-Vapor Mixture Back to Liquid:

$$a_s\left[\frac{g}{a^2}(H_s-H_{sv})+a_v\right]-(V-V_m)=0 \quad (7)$$

$$g(H_s-H_{sv})+(V-V_m)(V-V_m-a_s)=0 \quad (8)$$

- Equations for a Discrete Vapor Cavity:

$$\forall_{vc}=\int_{t_{in}}^{t}A(V-V_u)\,dt \quad (9)$$

In the DVCM algorithm, discrete vapor cavity equation is incorporated into the water hammer equations, while all seven coupled equations are solved for the GIVCM algorithm. It is important to remember that while these models certainly have their own advantageous when dealing with a mixture of liquids and gases, decomposing the fluid into two different species, without the explicit term for interfacial mass transfer is potentially problematic in distinguishing leak under slack flow conditions. [1]

A secondary class could be a novel model with the possibility to address phase change (slack, column-separation, cavitation, interfacial mass transfer rate) directly from its model.

In other words, the ability of the model to address phase change of the dominant liquid phase from liquid to vapor and from vapor to liquid comes first compared to designating different governing equations for different phases in that liquid, such as dissolved gases.

$$\frac{1}{c^2}\frac{\partial P}{\partial t}+\frac{\partial(\rho u)}{\partial x}=\sigma \quad (10)$$

$$\frac{D(\rho u)}{Dt}+\frac{\partial P}{\partial x}+\frac{(\rho_l-\rho_v)^2\rho_l f^*}{2D(\rho-\rho_v)}u|u|+\rho f_x-\beta=0 \quad (11)$$

Equations (10) and (11) describe the novel model which also solve for density along with the velocity and pressure as demonstrated in Figure 5.

Equation (10) is the continuity equation with the speed of sound and temporal pressure instead of density. Equation (11) is the transient momentum equation for a one-dimensional, unidirectional flow in the pipeline with variable density and friction factor used to represent the viscous losses. σ and β become zero if no injection or losses exist in the system.

In these equations, ρ is density, *u* is flow velocity, *P* is the pressure, *t* is time, and *c* is the speed of sound in the fluid.

The right-hand side of equation (10) is a non-zero term representing residual values during a leak incident.

By decomposing the second term in equation (10), the second term of equation (1), $\frac{\rho_l}{\pi r_0^2}\frac{\partial Q}{\partial x}$, appears and an additional term whose unit is mass flow rate per unit control volume,$u\frac{\partial \rho}{\partial x}$ This is the explicit term for interfacial mass transfer between vapor and liquid phase -of the same substance, water in here- which is can be taught of a density-difference term multiplied thermodynamical quality of the substance.

The other difference between equations (1) and (10) is in density terms. The subscript in equation (1) shows it is a designated liquid density value. In contrast, the density term in equation (10) can be the density of a mixture of the same substance during phase change. Also, velocity terms in equations (10) and (11) represent the difference between the same substance's phases' flow rates. More details on the novel model can be found in [1].

The novel model's superiority in synchrony with the actual transient events leading to column separation or slack compared to conventional models discussed in this paper are verified and validated [2].

Two selected models to compare the performance of the Leak Detection Systems under the presence of slack are the DVCM conventional model from the first and the novel model from the second class of the mode-based algorithms.

The novel model can address multiphase stemming from the phase change of the same substance between liquid and vapor phases directly from its explicit term in the mathematical model. Conventional Models usually either assign a secondary equation of mass balance and momentum balance for the gaseous phase or put artificial constraints in the flow chart of the numerical algorithm of the CPM model to consider mass transfer rate between that phases. (see Figure.4)

DESCRIPTION OF THE FLUID

Conventional models have a common characteristic in their description of the second phase or gaseous phase, and that is that the second phase is not the same substance as the primary liquid phase. Hence, as a separate substance, there is no need to consider it. However, consider the phase change of pure water without any dissolved gases in a pipeline and let the phase change be due to cavitation of the liquid from the liquid to vapor of the same substance to have a better picture of the needed interfacial mass transfer rate during phase changes of slack, evaporation, and condensation. We are assuming that water is degassed, and the only gaseous phase can come as vapor phase from the cavitation of the liquid phase. As it is shown in the Results section later, the initial calculations of the flowrates from the conventional method results in oscillatory values in some cases. Also, the conventional model does not solve for density causes an imbalance between the calculated flow rates at the system's boundaries, which can be interpreted as a leaking incident while it is not the case.

Therefore, two attempts to modify the initial results of the conventional CPM have been made before the final report of its performance. The oscillations in the flow rates are reduced by using the moving average of the values. The second modification is applied to resolve the false alarms as the result of the imbalance. We consider the average imbalance of the line and add it to the downstream flow rates. Both the novel and conventional CPMs are challenged to detect the leak during various operating conditions. Figure 2 demonstrates the operating conditions under which a leak test can be performed to evaluate the performance of the leak detection systems and their robustness. The operating conditions are categorized as steady-state, before shut-down, during shut-in and, before start-up to cover all possible operating conditions, a leak can happen. Figure 3 shows another possible transient operating condition caused by a sudden pressure drop in upstream.

DESCRIPTION OF THE EXPERIMENTS

The experimental tests were conducted on a flow loop with a schematic shown in Figure 1. The flow loop is a 374-m (1227 ft) long pipeline with a diameter of 88.9 mm (3.5 in), carrying water and shares geometric, kinematic, and dynamic similarities with the industrial scale pipelines.

The pipe is horizontal along its length except for 10 m (32.8 ft) of it which has an adjustable elevation profile to help with creating scenarios going through a phase change. This part of the line has a clear pipe to observe the bubbles. The properties of the pipe and fluid were presented in Table 1.

Data is collected from two pressure transmitters which are placed 156 m (512 ft) apart at the upstream and downstream of the elevated section of the pipe. A leak site is located 38 m (125 ft) before the elevated section for the inception of leaks of different rates.

Table 1- Properties of the pipe and fluid

Property:	**Value:**
Pipe outer diameter	88.9 mm (3.5 in)
Pipe wall thickness	5.5 mm (0.216 in)
Pipeline length	374 m (0.23 miles)
Pipe roughness	1.5 μm (6×10^{-5} in)
Pipe Young Modulus of elasticity	3.3 GPa (4.8×10^{5} psi)
Density	997 kg/m^3 (62.2lb/ft^3)
Viscosity	8.9×10^{-4} Pa.s (0.89 cP)
Vapor Pressure	3.42 kPa (0.5 psi)
Bulk modulus of elasticity	1.86 GPa (2.7×10^{5} psi)

Table 2 summarized 14 cases studied in this paper to elaborate on the effects of phase change on the performance of the leak detection systems. As described in the second column of Table 2, the operating condition during which the leak has occurred was steady state for cases 1 to 8 and transient for the rest of them. Leak begins a few minutes after the pump stopped, during the shut-in, for cases 9 and 10.

The leak valve has been opened right before the pump shut-down for cases 11 and 12, and right before the start-up for cases 13 and 14. The elevation peak was adjusted to let us perform the tests at three different levels- flat, 12.59 m (41.31 ft), and 15.59 m (51.15 ft). A variety of leak rates were obtained depending on the established flowrate of the line and the leak valve opening percentage during each test as reported in the third column of Table 2.

The last column of Table 2 reports the presence of slack in the pipe. The first and the second digit in the bracket show whether the vapor phase is present (1) or not (0) before and after the leak initiation, respectively.

Table 2- Summary of the cases

CASE NO.	Operating condition at leak time	Elevation Peak m (ft)	Leak rate Lit/min (ft^3/min)	Slack [before leak - after leak]
1	steady state	0 (0)	42.2 (1.49)	[0--0]
2	steady state	15.59 (51.15)	43.9 (1.55)	[1--1]
3	steady state	0 (0)	47.7 (1.68)	[0--0]
4	steady state	15.59 (51.15)	49.6 (1.75)	[1--1]
5	steady state	12.59 (41.31)	24 (0.85)	[1--1]
6	steady state	15.59 (51.15)	18.4 (0.65)	[1--1]
7	steady state	12.59 (41.31)	21.7 (0.77)	[1--0]
8	steady state	15.59 (51.15)	12.8 (0.45)	[1--1]
9	Shut-In	12.59 (41.31)	14.8 (0.52)	[1--0]
10	Shut-In	15.59 (51.15)	14.8 (0.52)	[1--1]
11	Shut-down	12.59 (41.31)	15.4 (0.54)	[1--0]
12	Shut-down	15.59 (51.15)	15.4 (0.54)	[1--1]
13	Start-Up	12.59 (41.31)	22.9 (0.81)	[1--1]
14	Start-Up	15.59 (51.15)	21.4 (0.76)	[1--1]

RESULTS

It is clear in the top section of Figures 7, 9, 11, 13, 15, 17, 19, 21, 23, 25, 27, 29, 31, and 33 that without modifications, there is an imbalance in the flowrates from the conventional model before leak results in generating the false alarms.

The leak will be missed in cases 4, 5, and 10 -14, mostly caused by the oscillatory response of the conventional model. After the modifications of the calculated flowrates by Conventional CPM, the results for such modification are presented in the bottom plots of Figures 6, 8, 10, 12, 14, 16, 18, 20, 22, 24, 26, 28,30, and 32.

The pressure changes, the flow rate of Novel CPM, and modified flow rates of conventional CPM for each 14 cases were demonstrated in Figures 6, 8, 10, 12, 14, 16, 18, 20, 22, 24, 26, 28,30, and 32. The top plot of these figures shows the pressure vs. time from the PITs located at the upstream (black line) and downstream (red line) of the section of the pipe under study. The middle plot shows the flow rate values vs time calculated by novel CPM. The solid black line and solid red line are the flowrates from the novel model at the upstream and downstream, respectively. The plot at the bottom demonstrates the flow rates of the conventional CPM after the application of the modifications. The blue dashed line and the yellow dashed line are the flow rates from the conventional model upstream and downstream, respectively. The top section of Figures 7, 9, 11, 13, 15, 17, 19, 21, 23, 25, 27, 29, 31, and 33 show the flow rates from Novel and Conventional CPM as calculated by these CPM before any modifications. At the bottom, the fluid density at the elevation peak over time is plotted as it changes when the phase change occurs.

Except for case 1 and case 3 with a flat elevation profile, phase change happened at time(s) during the rest of the cases. The vapor phase was present either in the form of the dispersed or elongated bubbles in the liquid continuum. For example, as shown in the bottom plots of Figures 17, 21, and 33, the density at the peak drops to the vapor density showing the vapor phase fully filled the pipe at the peak for cases 6, 8, and 14.

Table 3 represents the leak detection system (LDS) results for novel and conventional models before and after the leak. True-negative (TN) means that no alarm is generated by the leak detection system when there is no leak. False-positive (FP) refers to the cases in which false alarms happened. True-positive (TP) is for the times that LDS correctly alarms as the leak is happening. False-negative (FN) means that LDS missed the leak and failed to report it.

Table 3- Results of the leak detection system before modifications

CASE NO.	Before leak Novel / Conventional	After leak Novel / Conventional
1	TN / TN	TP / TP
2	TN / FP	TP / TP
3	TN / TN	TP / TP
4	TN / FP	TP / FN
5	TN / FP	TP / FN
6	TN / FP	TP / TP
7	TN / FP	TP / TP
8	TN / FP	TP / TP
9	TN / FP	TP / TP
10	TN / FP	TP / FN
11	TN / FP	TP / FN
12	TN / FP	TP / FN
13	TN / FP	TP / FN
14	TN / FP	TP / FN

As it can be seen in Table 4, the applied modifications caused all false alarms generated by the conventional models to be resolved. However, in general, find the correct value to treat the imbalance can result in masking a leak from being detected as this is the case for the false negative (FN) alarms for the conventional model after the leak in cases 4, 5, and 8-14.

Table 4- Results of the leak detection system after modifications

CASE NO.	Before leak Novel / Conventional	After leak Novel / Conventional
1	TN / TN	TP / TP
2	TN / TN	TP / TP
3	TN / TN	TP / TP
4	TN / TN	TP / FN
5	TN / TN	TP / FN
6	TN / TN	TP / TP
7	TN / TN	TP / TP
8	TN / TN	TP / FN
9	TN / TN	TP / FN
10	TN / TN	TP / FN
11	TN / TN	TP / FN
12	TN / TN	TP / FN
13	TN / TN	TP / FN
14	TN / TN	TP / FN

For example, in Figure 28 and Figure 30, resolving the imbalance before the leak also results in reducing the imbalance as the leak happens in such a way that makes it hard for the leak detection to recognize it and alarm.

ANALYSIS AND DISCUSSIONS

Two outcomes for each class of algorithms before and after the leak in Tables 3 and 4 allow for comparing the results as three separate sets of a binary classification test, which compares sensitivity and specificity quantitatively as global statistical measures of the performance.

$$Sensitivity = \frac{Number\ of\ TP}{Number\ of\ TP + Number\ of\ FN} \quad (12)$$

$$Specificity = \frac{Number\ of\ TN}{Number\ of\ TN + Number\ of\ FP} \quad (13)$$

True Positive (TP): An alarm correctly is generated for a leak incident.

False Positive (FP): An alarm is generated incorrectly identified as a leak.

True Negative (TN): Alarm is avoided during a leak-free period.

False Negative (FN): The alarm is not generated for a real leak.

The possibility of non-sense results for these methods at each given grid point in a finite difference approach using the characteristics is shown in Figure 36. The artificial constraint in their flow charts is due to the absence of an explicit term in their model to take care of phase change from liquid to vapor and vice versa. Hence, a development to the conventional approaches is needed when slack and its whereabouts are a concern.

CONCLUSIONS

RTTM CPM models which do not have a way to ensure and assure their temporal and spatial predictions when it comes to slack operating conditions are not reliable as the basic algorithms for leak detection systems. This is due to the fact that missing the opportunity of solving the field of density in real-time suppresses the multiphase nature of the phase change to enter the governing equations of the model being solved and therefore the inference engine of the CPM system makes impartial calculated data. This incapability in providing calculated data about the density in real-time makes the alert algorithm faulty in action as it can neither distinguish the slack from a leak by itself nor, it can always use the instrument data for that purpose. Without the explicit term for interfacial mass transfer rate, the 'calculated data' does not allow for the solution of phase change in terms of inception and evolution to occur seamlessly and synchronized with the physical pipeline and hence is not the best quality 'calculated data' to be transferred from the PDE module to the Alarm Generation Module of the CPM system. (see Figure 4). The best 'calculated data' comes from an algorithm that solves a type of PDE model that allows for the phase change in terms of inception and evolution seamlessly and synchronized with the physical pipeline.

A summary of conclusions:

- Slack can mask the leak or produce frequent false alerts.
- Same LDS makes wrong decisions due to impartial calculated data.
- Reliability and Robustness for CPM-based LDS are shown to be fully compromised without a real-time solution of the density field.

ACKNOWLEDGMENT

The authors would like to acknowledge the help of our colleagues in India, Mygapula SubbaRao, Director of EnggVille Innovations Pvt. Ltd. and the Intern, Mygapula Aneeth with the built of the designed flow-loop and the PSIG board members Rick Brown, Ivor Ellul, and Ed Nicholas for their comments and valuable feedback on the initial and final drafts of this paper.

REFERENCES

1. Ghasvari Jahromi H, Ekram F, Roxas M, Mokamati S. "A Mathematical Model for the Spatial Prediction and Temporal Evolution of the Column Separation in a Flowing Hydrocarbon Transmission Pipeline." Paper presented at the PSIG Annual Meeting, London, UK, May 2019. Paper Number: PSIG-1910.

2. Ghasvari Jahromi H, Roxas M, Mokamati S. "Column Separation in a Shut-In Liquid Hydrocarbon Transmission Pipeline." Proceedings of the 2018 12th International Pipeline Conference. Volume 3: Operations, Monitoring, and Maintenance; Materials and Joining. Calgary, Alberta, Canada. September 24–28, 2018. V003T04A027. ASME.

3. Stanley G. "Sensitivity Study for Leak Detection in Slack Line Conditions." Paper presented at the PSIG Annual Meeting, San Antonio, Texas, November 2005.

4. Geiger G, Vogt D. "A Combined Leak Detection Method Using Pattern Recognition Techniques." Proceedings of the 2014 10th International Pipeline Conference. Volume 1: Design and Construction; Environment; Pipeline Automation and Measurement. Calgary, Alberta, Canada.

5. Lu Z, She Y, Loewen M. "A Sensitivity Analysis of a Computer Model-Based Leak Detection System for Oil Pipelines." *Energies*.2017;10(8):1226.

6. Jian-Jun Shu, Modelling vaporous cavitation on fluid transients, International Journal of Pressure Vessels and Piping, Volume 80, Issue 3, 2003, Pages 187-195, ISSN 0308-0161,

7. API 1130, 2007 Edition, September 2007- Computational Pipeline Monitoring for Liquid Pipelines

8. Bergant, Anton & Simpson, Angus. (1999). Pipeline Column Separation Flow Regimes. Journal of Hydraulic Engineering.125.10.1061/(ASCE)0733-9429 125:8(835).

AUTHOR BIOGRAPHY

Hamed Ghasvari Jahromi Chief (R&D) Scientist has 10+ years of experience developing and applying mathematical models and fluid dynamics theories to Industrial Problems. He has extensive experience developing leak detection technologies, especially column separation prediction models, RTTM, pattern recognition, computational fluid dynamics (CFD) for modeling and analysis in various applications in multi-phase flows (oil/gas/sediments), Cavitation modeling, pipeline flow modeling, and Transient flows. He authored research articles in peer-reviewed journals and has presented research projects at various international conferences. At Vanmok, he leads innovative engineering approaches by creating accurate mathematical models and developing robust numerical algorithms to solve the pipeline leak/theft detection models, Pipeline Simulations, and new methods of Leak detection and testing in accordance or beyond regulatory requirements.

Fatemeh Ekram (R&D) Scientist experienced in process control and data analytics. Currently, she is working on developing estimators and diagnostic algorithms for pipeline leak detection systems. Fatemeh got her B.Sc. & M.Sc. degrees from Sharif University of Technology and completed her Ph.D. at the University of British Columbia in Chemical Engineering.

Michael Roxas Simulation and Modelling Analyst has broad experience in pipeline leak detection, simulation, and modeling. Obtained a BSc. degree in Chemical Engineering from the University of Alberta. Michael's expertise includes experience in hydraulics modeling, pipeline simulations, pipeline leak detection testing, and software development.

Waqar Ali Mechanical Engineer (R&D) E.I.T
has knowledge of fluid mechanics, heat transfer, and thermodynamics. He also has a broad understanding of the ISO 9001:2015 Quality Management System (QMS). Obtained Bachelor of Science (BSc) in Mechanical Engineering from the University of Alberta. Waqar has been assisting the R&D team to perform experimental tests for writing research papers and to manage pipeline data used for experimental analysis.

Satya Mokamati Principal Engineer has broad pipeline leak detection, simulation, and modeling experience. Obtained Ph.D. in Mechanical Engineering from UBC, Vancouver; MS in Mechanical Engineering from UNB, Fredericton; Undergrad from India. Satya's expertise includes experience in hydraulics-modeling/ numerical analysis, Pipeline Simulations, Pipeline Leak Detection Testing, leak detection technology development.

FIGURES

Figure 1- Schematic of the flow loop

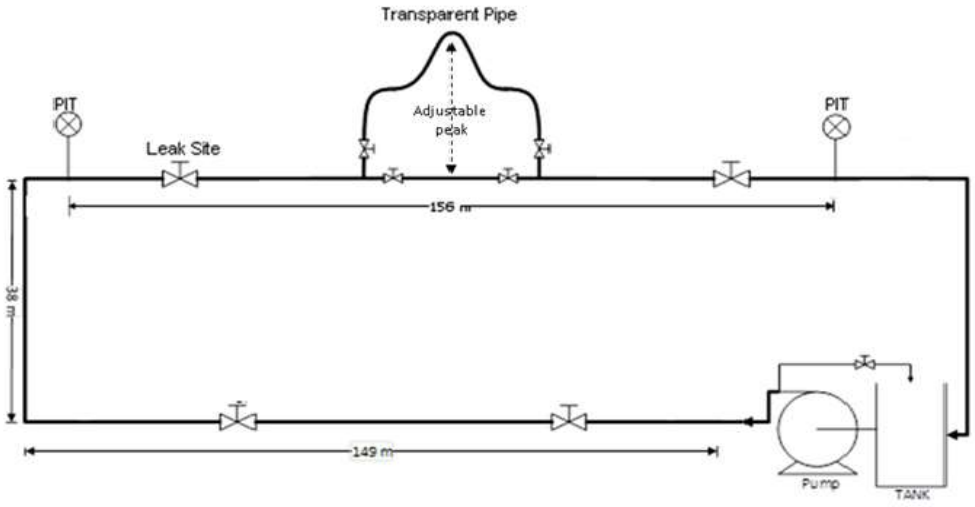

Figure 2- Choices of operational conditions for performing leak test (I)

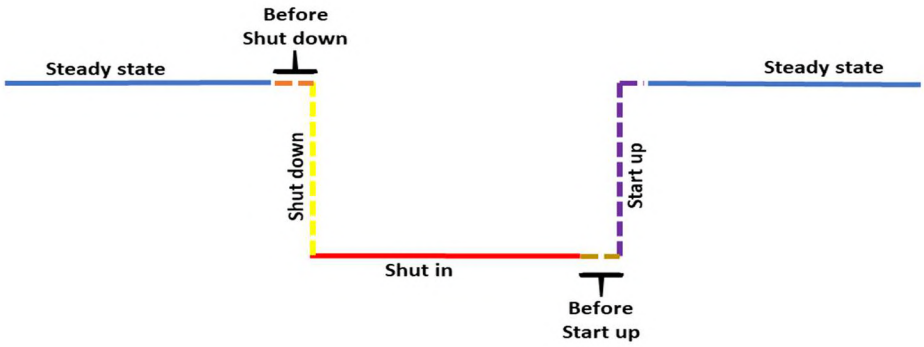

Figure 3- Choices of operational conditions for performing leak test (II)

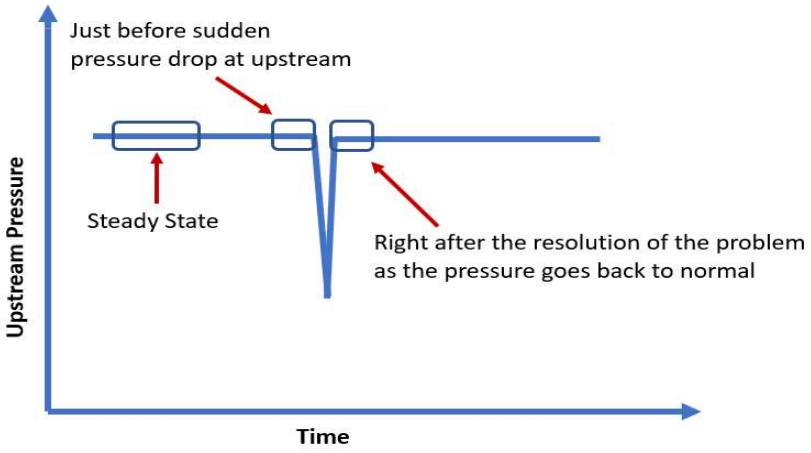

Figure 4- Architecture of usual CPM-based Leak Detection Algorithms used as LDS.

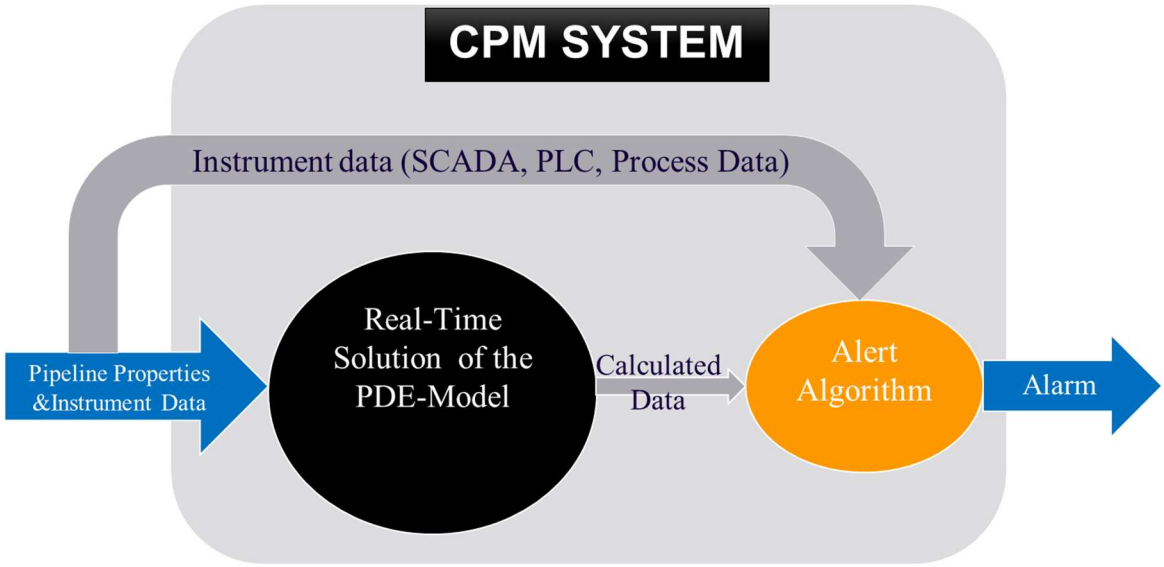

Figure 5- Calculated data comes from the numerical solution of the model's governing equations.

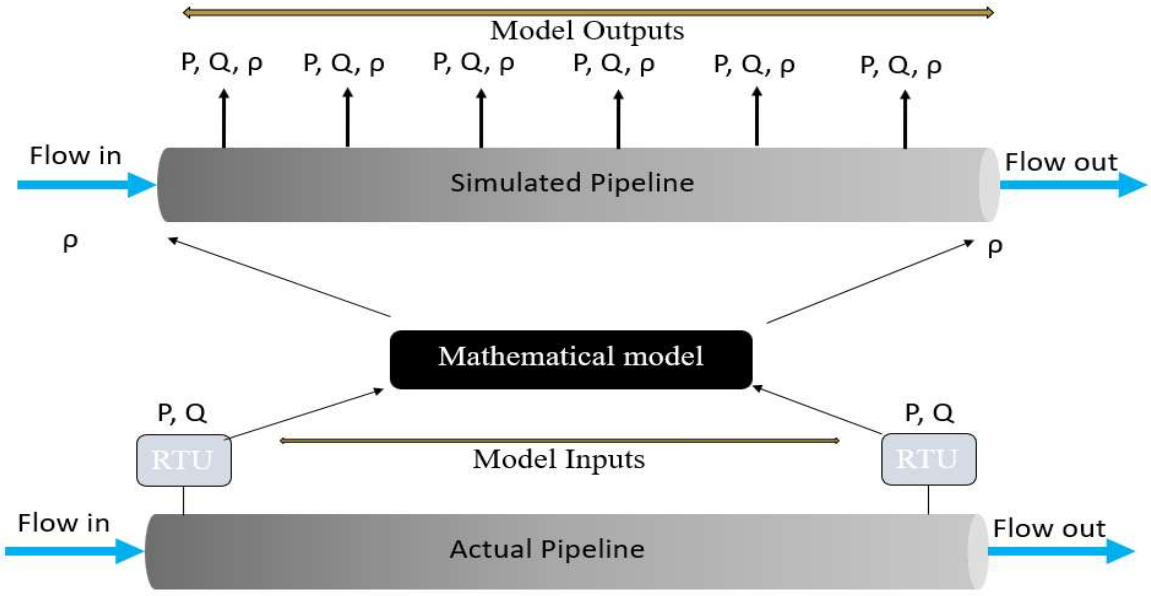

Figure 6- CASE NO. 1

(Top: pressures from PITs, Middle: flowrates of Novel CPM, Bottom: Modified flowrate of Conventional CPM)

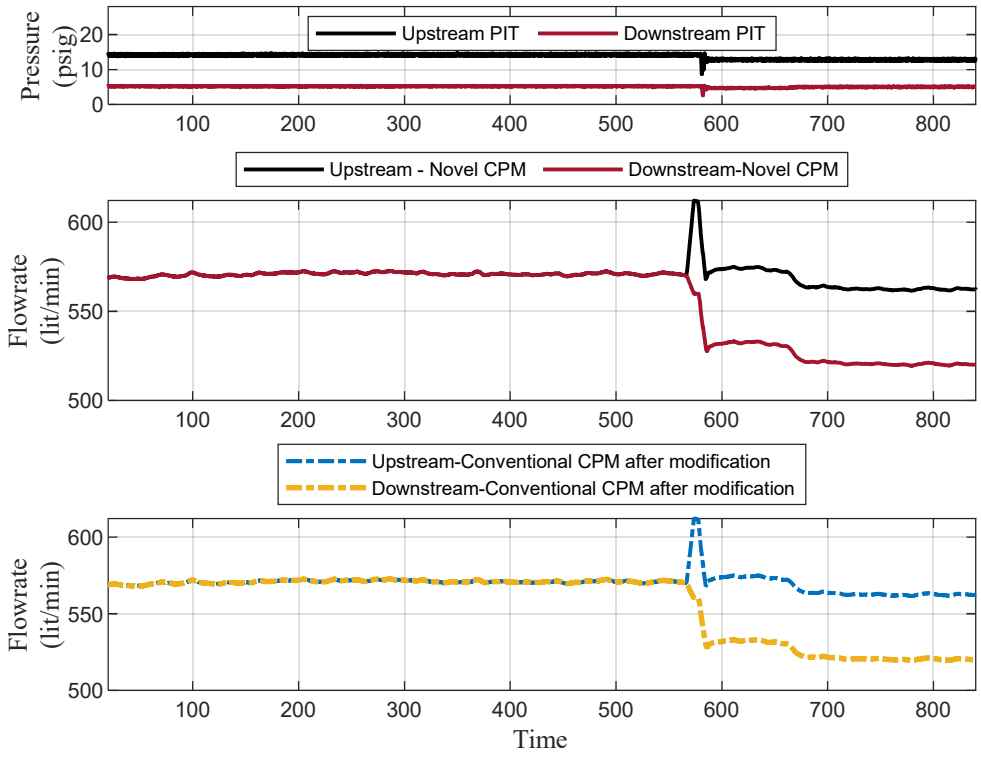

Figure 7- CASE NO. 1

(Top: flowrates of Novel CPM and Conventional CPM without modification, Bottom: changes of the density at the peak)

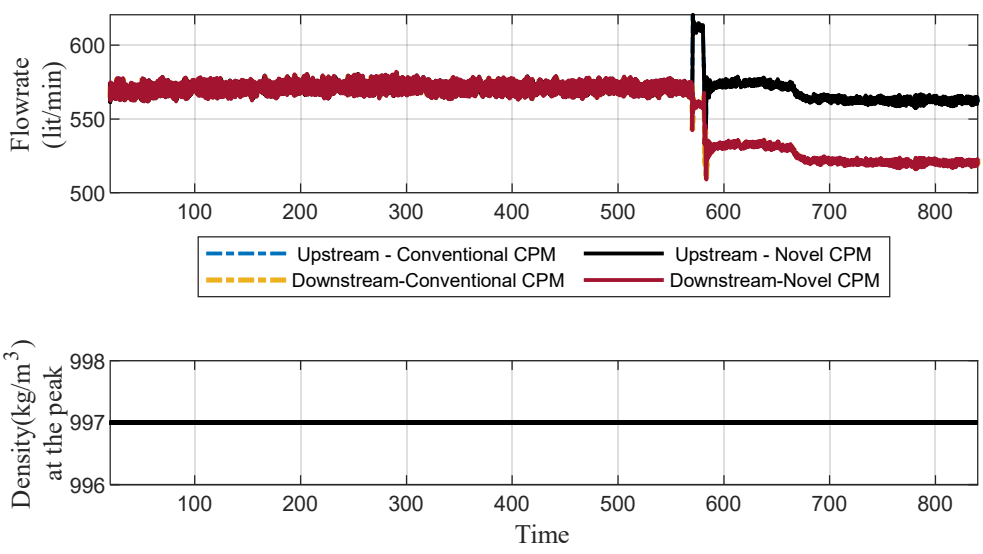

Figure 8- CASE NO. 2

(Top: pressures from PITs, Middle: flowrates of Novel CPM, Bottom: Modified flowrate of Conventional CPM)

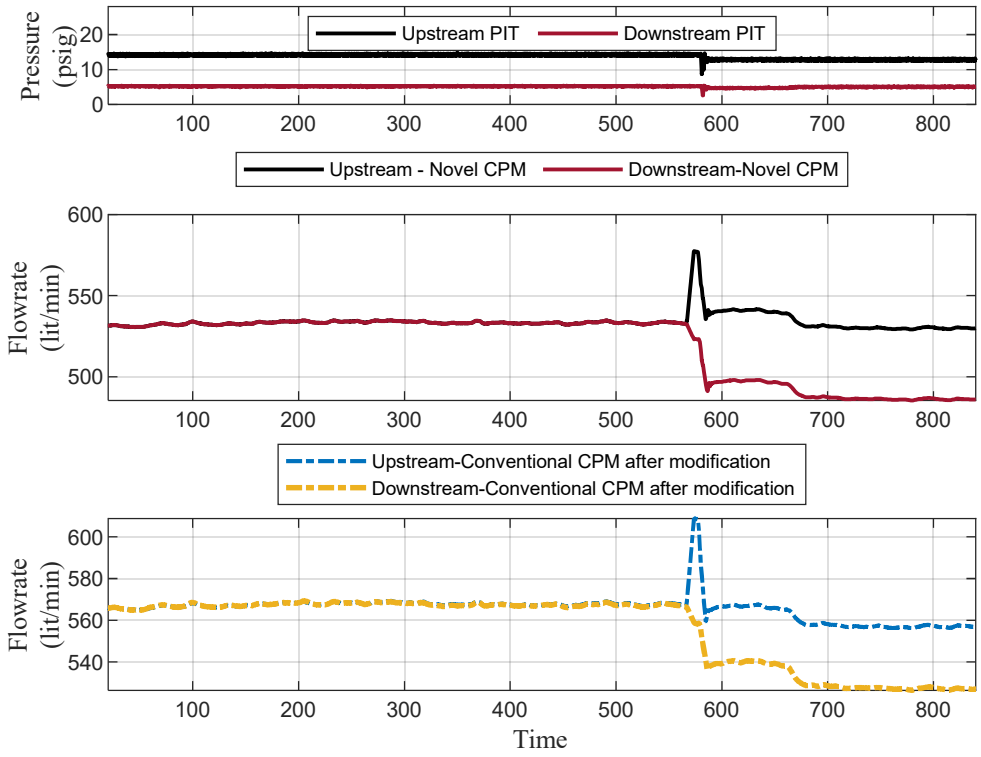

Figure 9- CASE NO. 2

(Top: flowrates of Novel CPM and Conventional CPM without modification, Bottom: changes of the density at the peak)

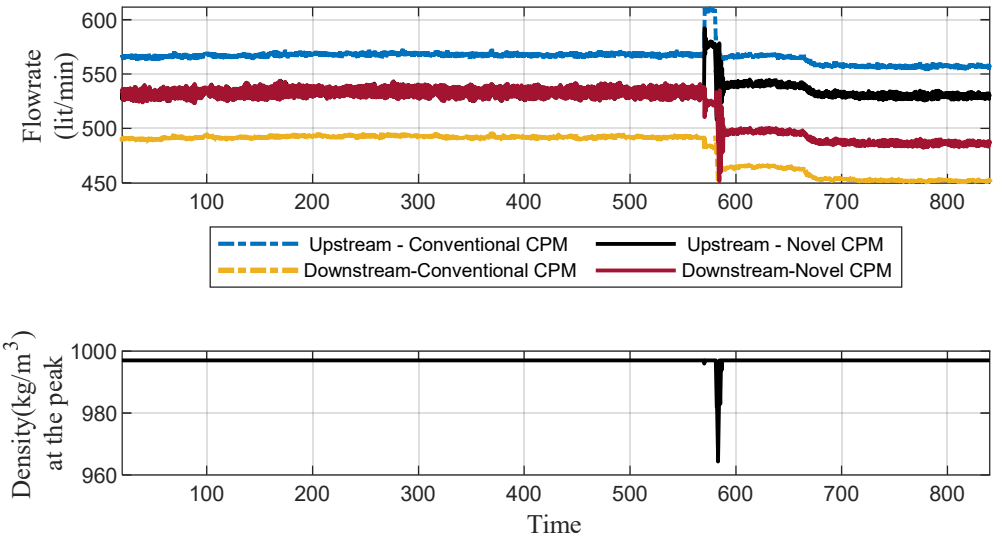

Figure 10- CASE NO.3

(Top: pressures from PITs, Middle: flowrates of Novel CPM, Bottom: Modified flowrate of Conventional CPM)

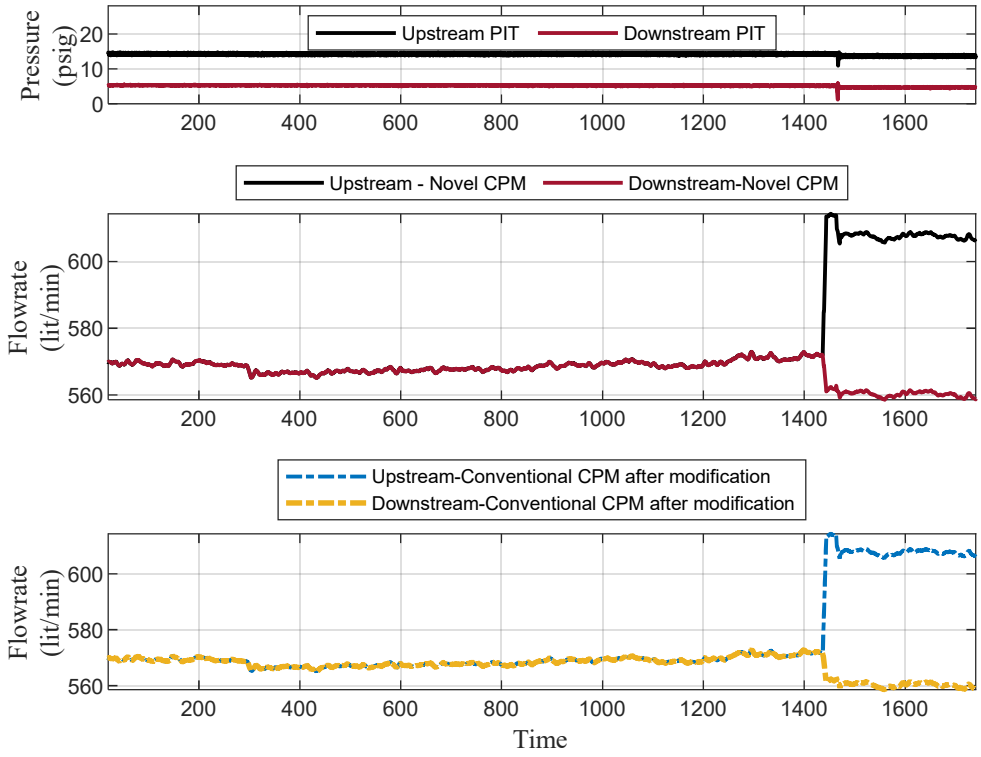

Figure 11- CASE NO.3

(Top: flowrates of Novel CPM and Conventional CPM without modification, Bottom: changes of the density at the peak)

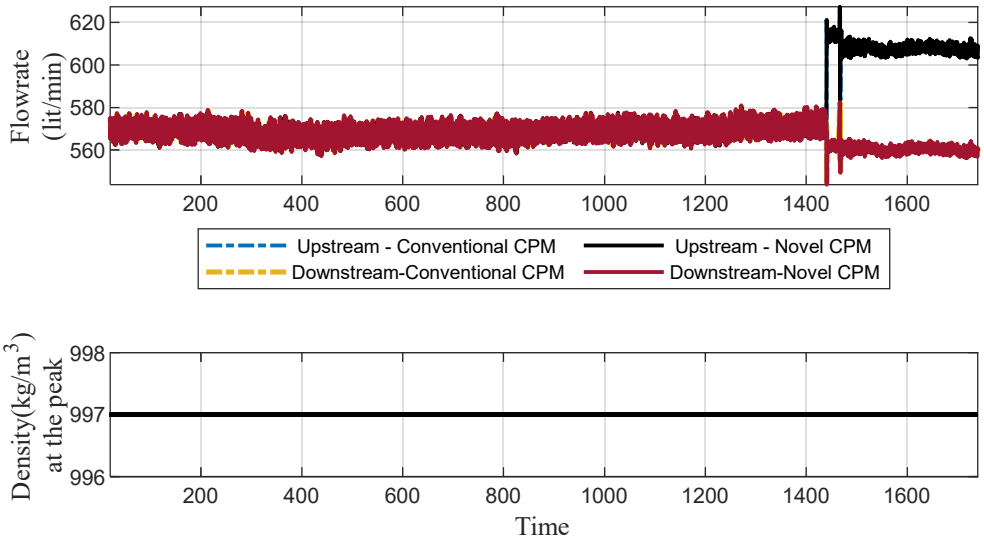

Figure 12- CASE NO. 4

(Top: pressures from PITs, Middle: flowrates of Novel CPM, Bottom: Modified flowrate of Conventional CPM)

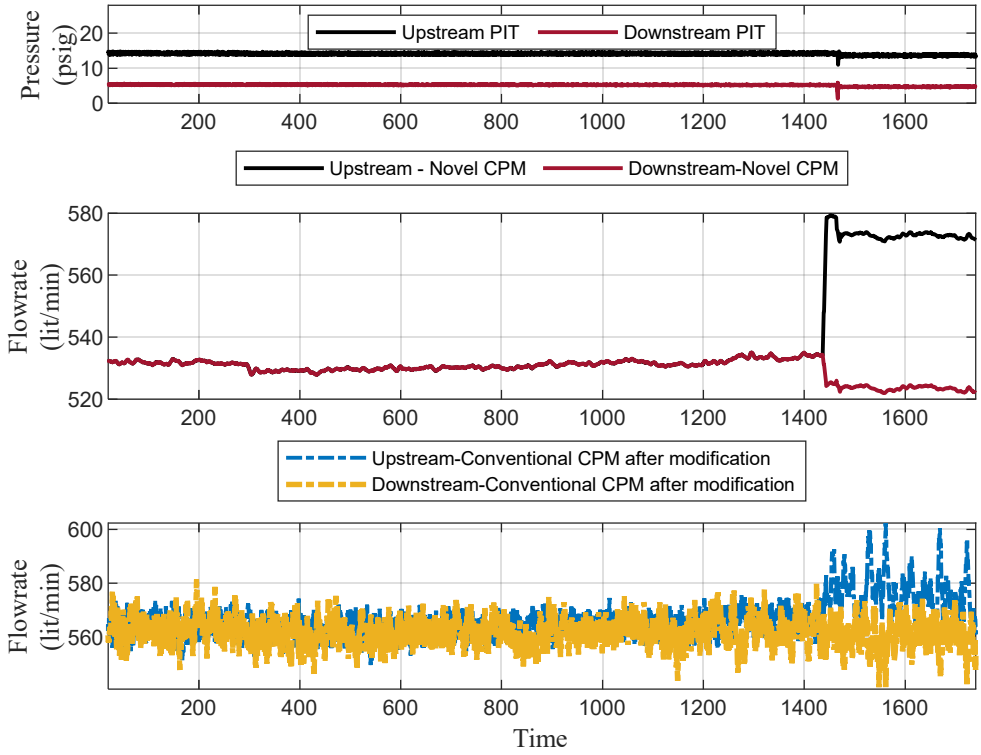

Figure 13- CASE NO. 4

(Top: flowrates of Novel CPM and Conventional CPM without modification, Bottom: changes of the density at the peak)

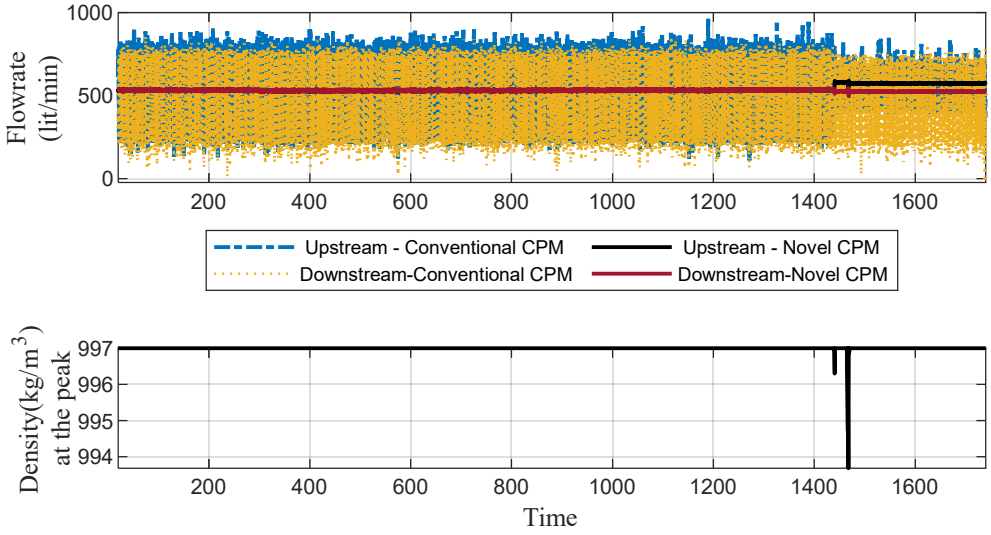

Figure 14- CASE NO. 5

(Top: pressures from PITs, Middle: flowrates of Novel CPM, Bottom: Modified flowrate of Conventional CPM)

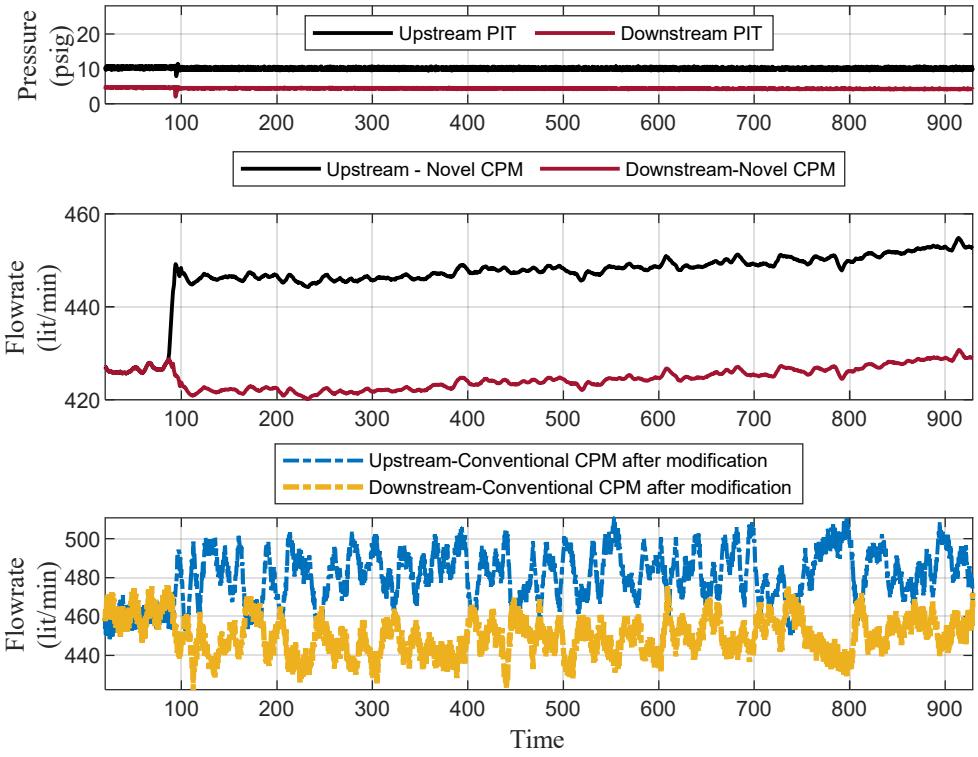

Figure 15- CASE NO. 5

(Top: flowrates of Novel CPM and Conventional CPM without modification, Bottom: changes of the density at the peak)

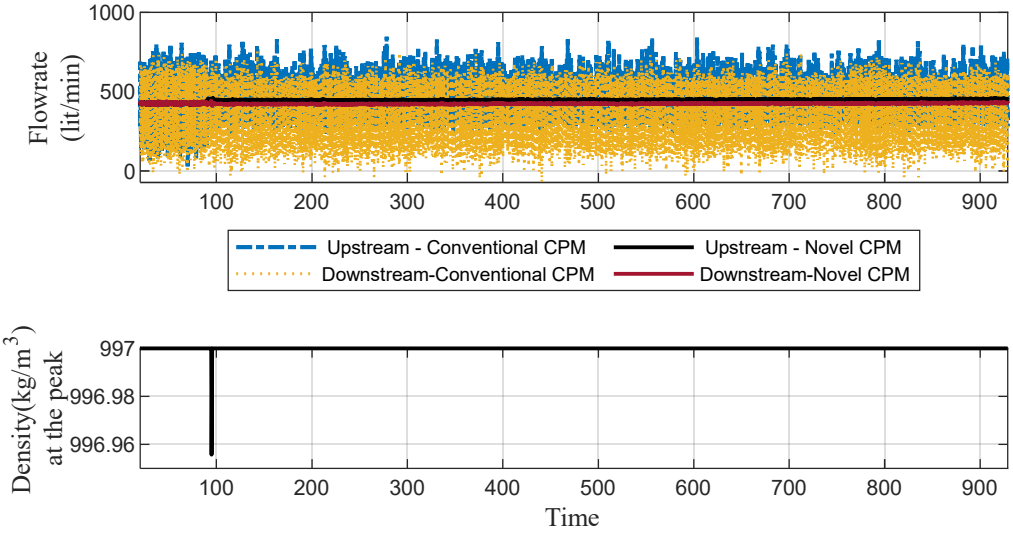

Figure 16- CASE NO. 6

(Top: pressures from PITs, Middle: flowrates of Novel CPM, Bottom: Modified flowrate of Conventional CPM)

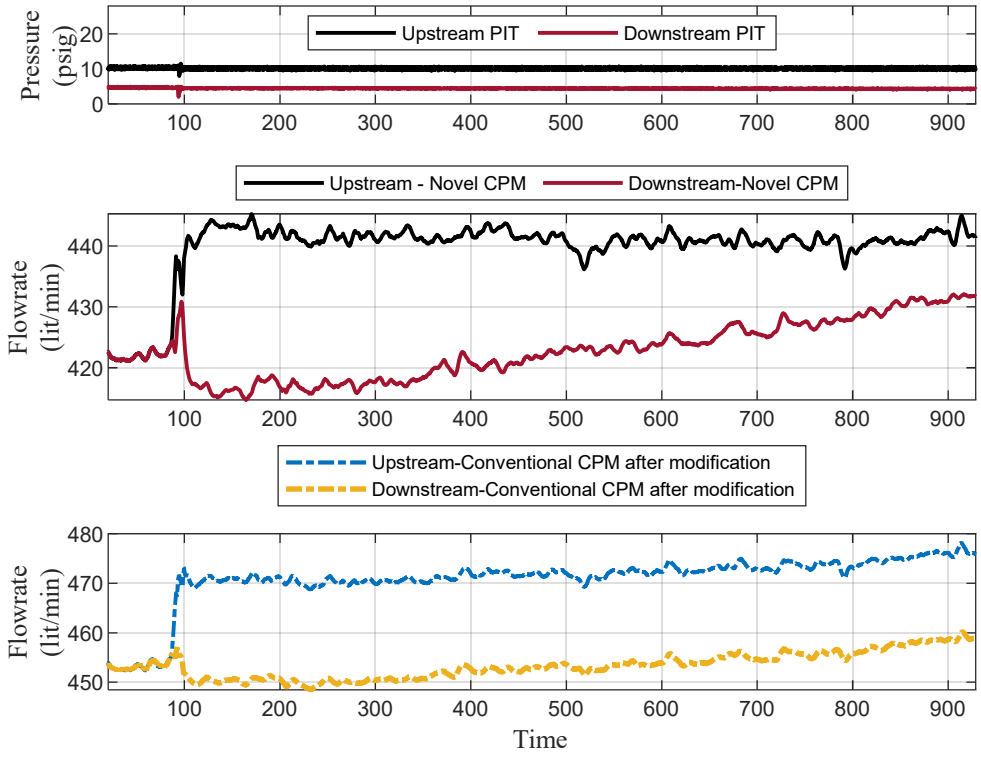

Figure 17- CASE NO. 6

(Top: flowrates of Novel CPM and Conventional CPM without modification, Bottom: changes of the density at the peak)

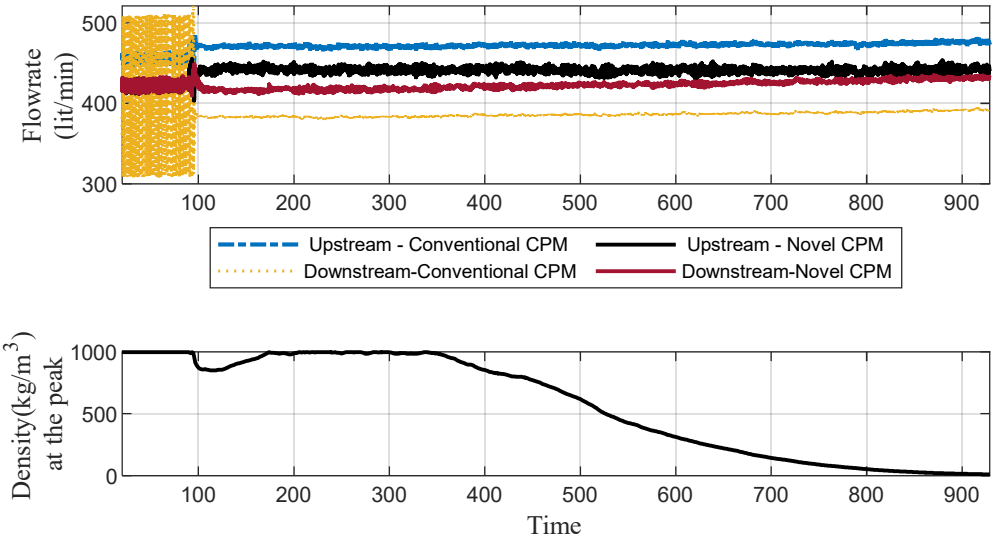

Figure 18- CASE NO. 7

(Top: pressures from PITs, Middle: flowrates of Novel CPM, Bottom: Modified flowrate of Conventional CPM)

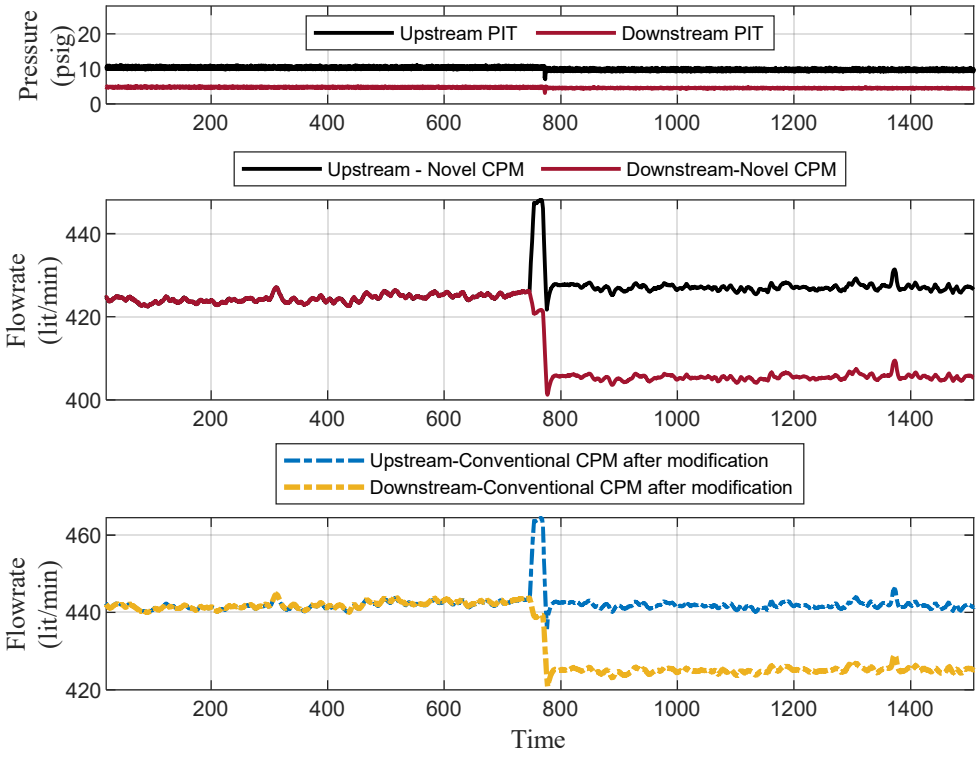

Figure 19- CASE NO. 7

(Top: flowrates of Novel CPM and Conventional CPM without modification, Bottom: changes of the density at the peak)

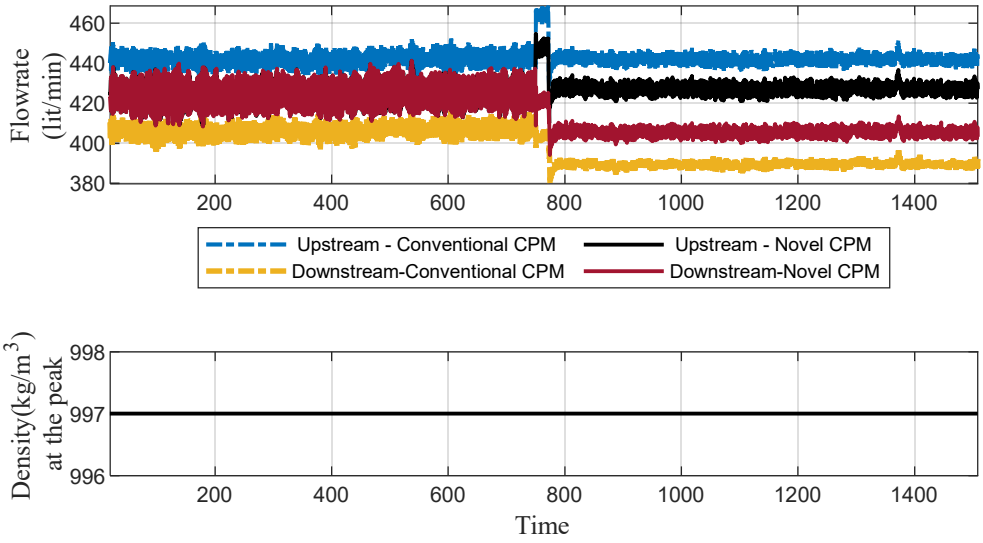

Figure 20- CASE NO. 8

(Top: pressures from PITs, Middle: flowrates of Novel CPM, Bottom: Modified flowrate of Conventional CPM)

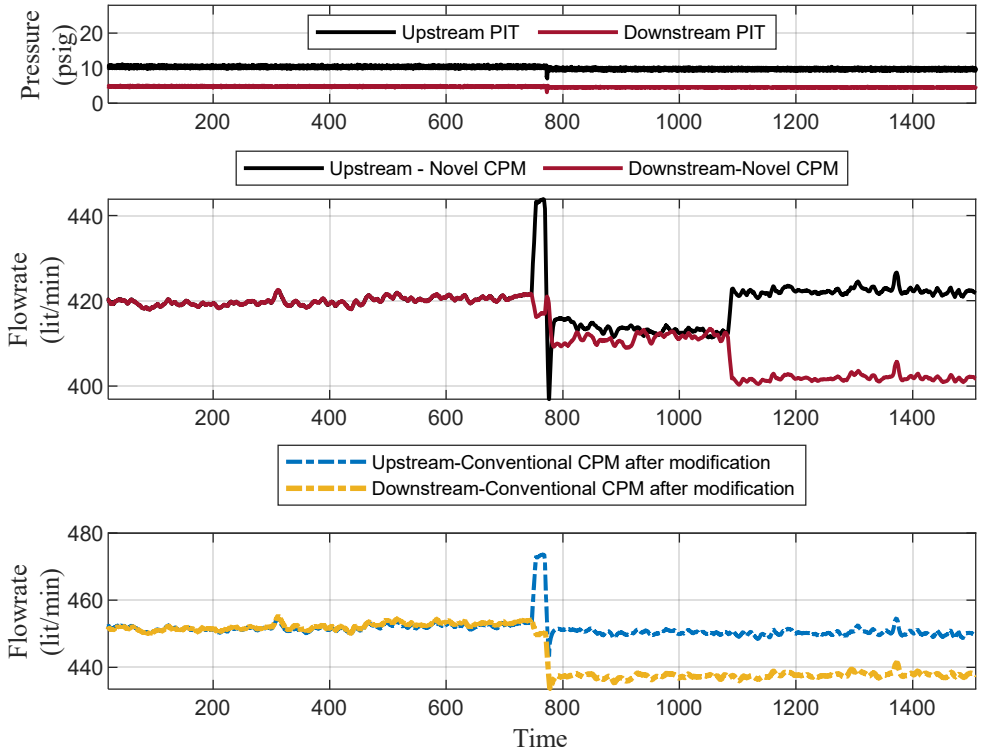

Figure 21- CASE NO. 8

(Top: flowrates of Novel CPM and Conventional CPM without modification, Bottom: changes of the density at the peak)

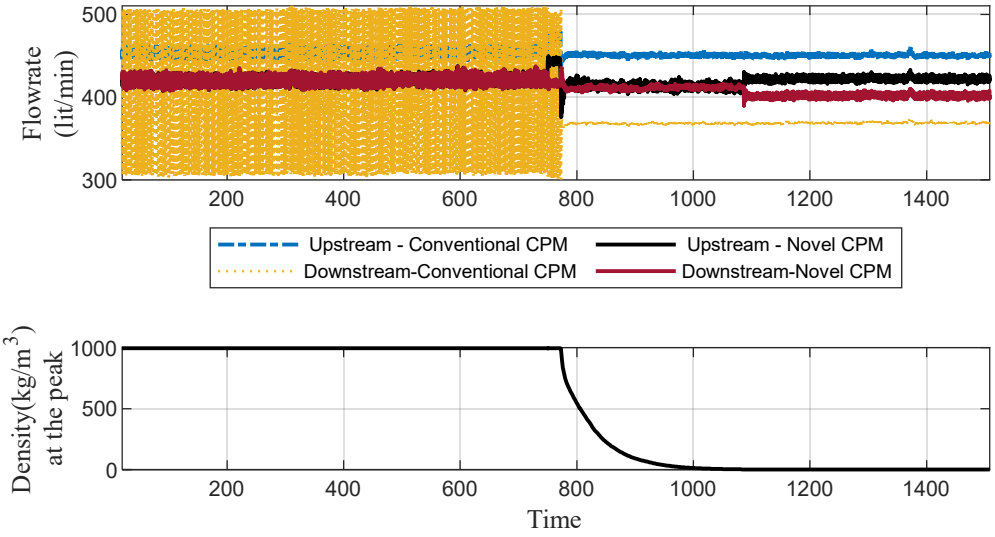

Figure 22- CASE NO. 9

(Top: pressures from PITs, Middle: flowrates of Novel CPM, Bottom: Modified flowrate of Conventional CPM)

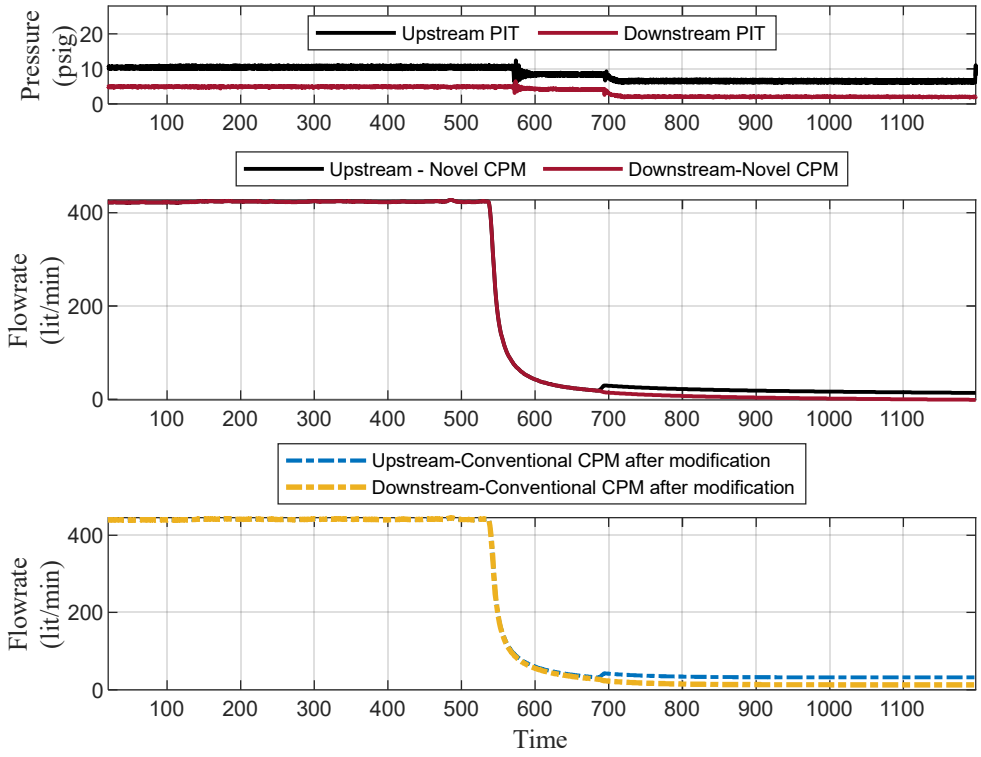

Figure 23- CASE NO. 9

(Top: flowrates of Novel CPM and Conventional CPM without modification, Bottom: changes of the density at the peak)

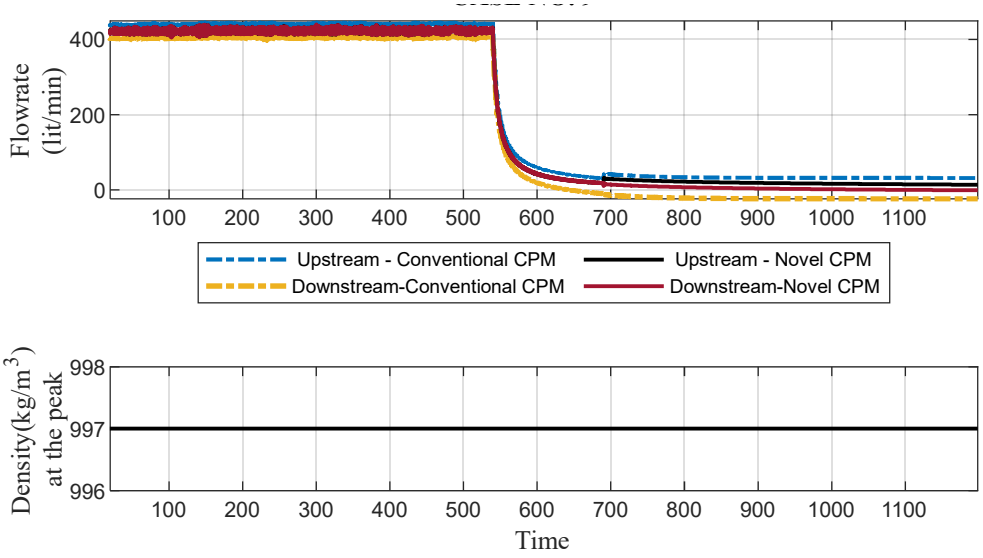

Figure 24- CASE NO. 10

(Top: pressures from PITs, Middle: flowrates of Novel CPM, Bottom: Modified flowrate of Conventional CPM)

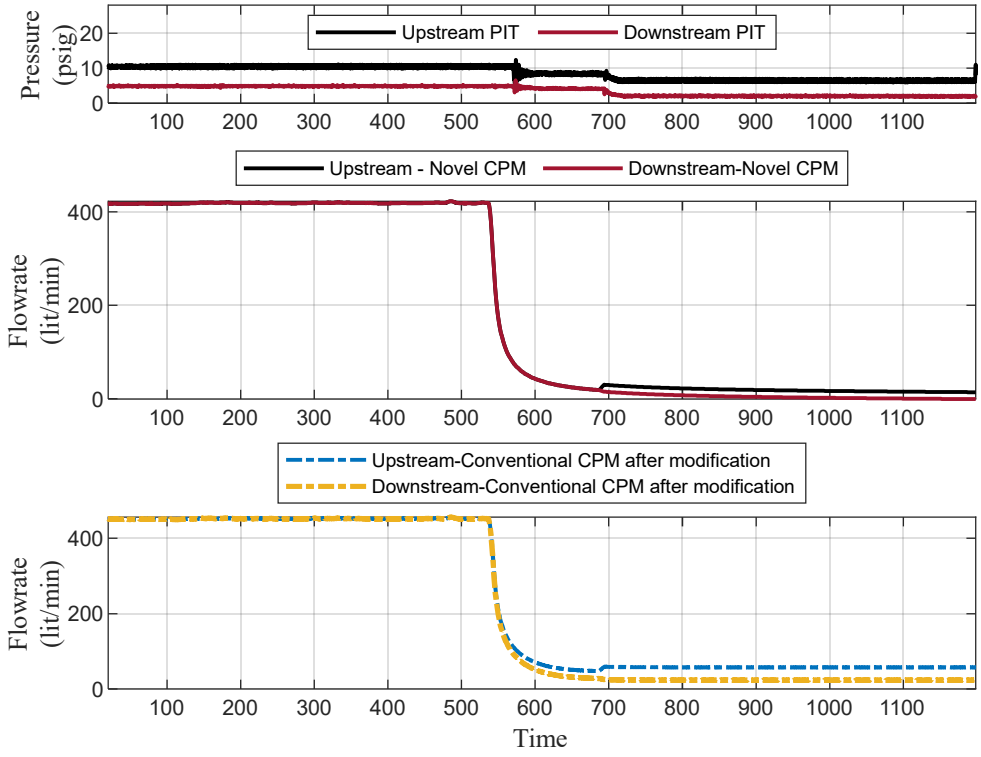

Figure 25- CASE NO. 10

(Top: flowrates of Novel CPM and Conventional CPM without modification, Bottom: changes of the density at the peak)

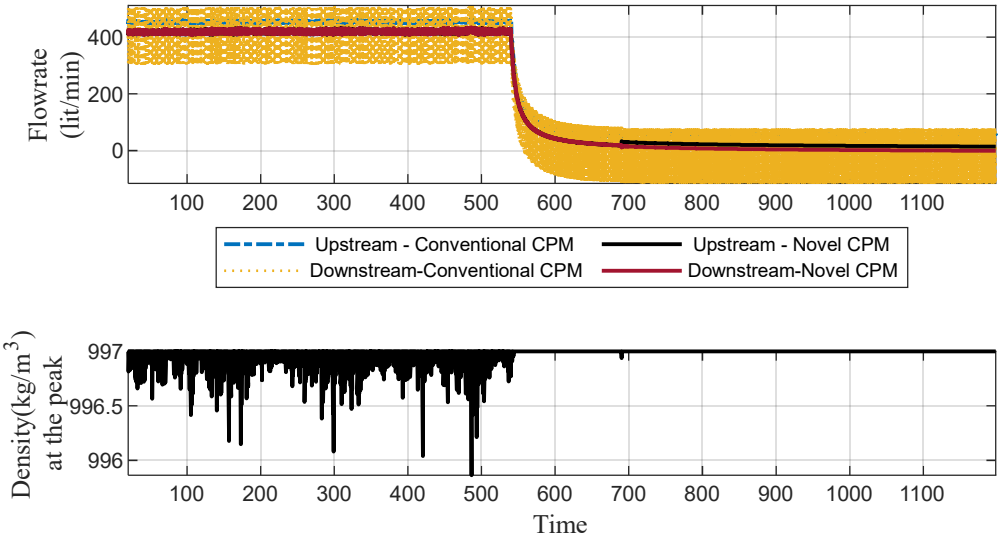

Figure 26- CASE NO. 11

(Top: pressures from PITs, Middle: flowrates of Novel CPM, Bottom: Modified flowrate of Conventional CPM)

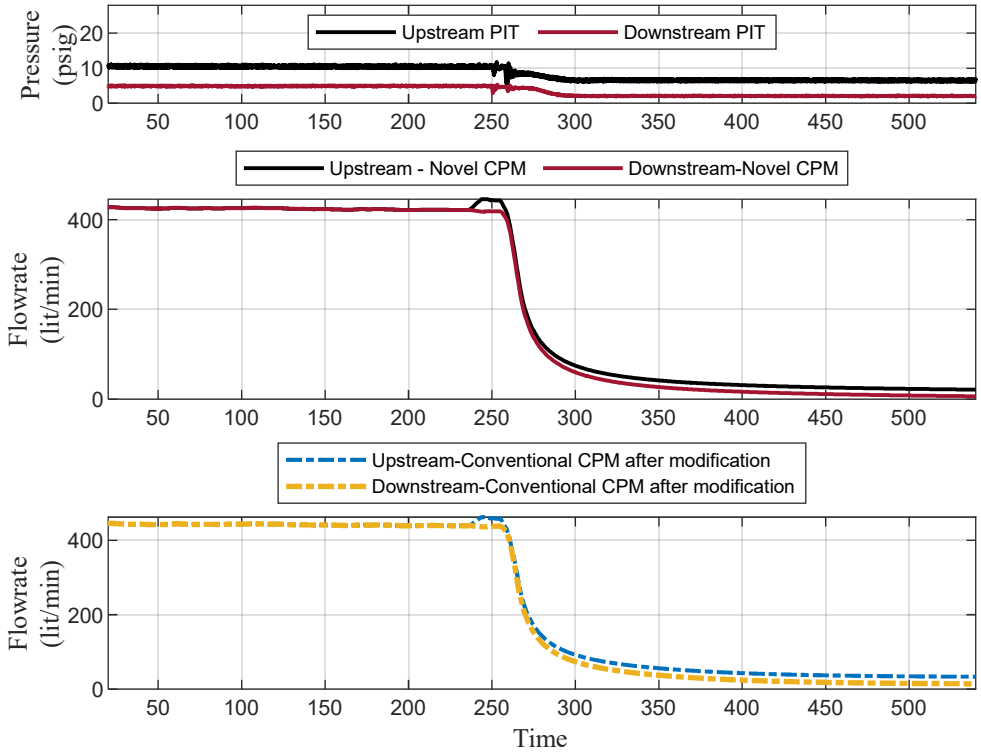

Figure 27- CASE NO. 11

(Top: flowrates of Novel CPM and Conventional CPM without modification, Bottom: changes of the density at the peak)

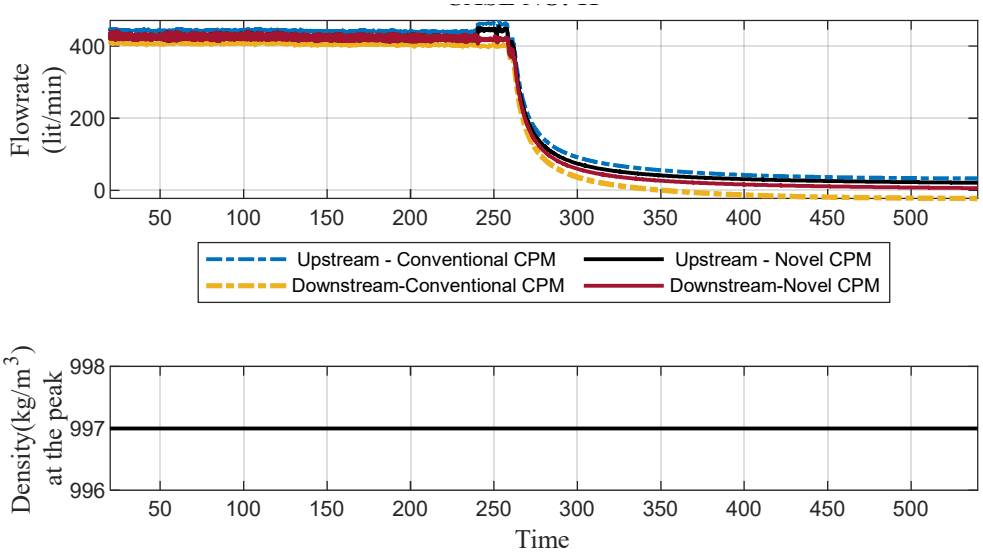

Figure 28- CASE NO. 12

(Top: pressures from PITs, Middle: flowrates of Novel CPM, Bottom: Modified flowrate of Conventional CPM)

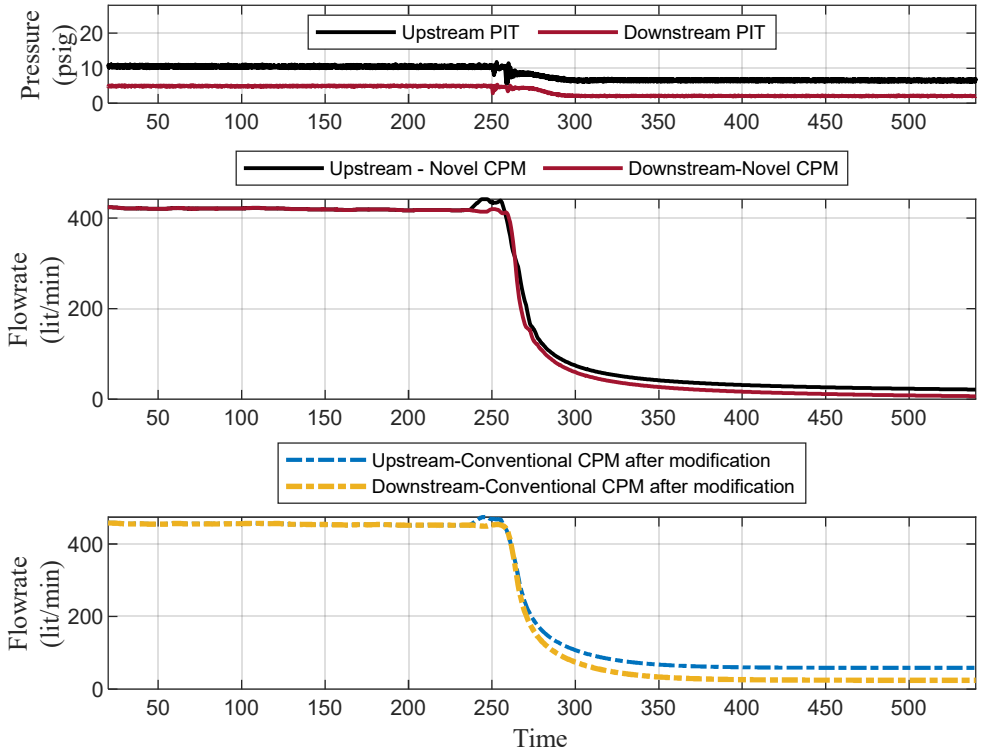

Figure 29- CASE NO. 12

(Top: flowrates of Novel CPM and Conventional CPM without modification, Bottom: changes of the density at the peak)

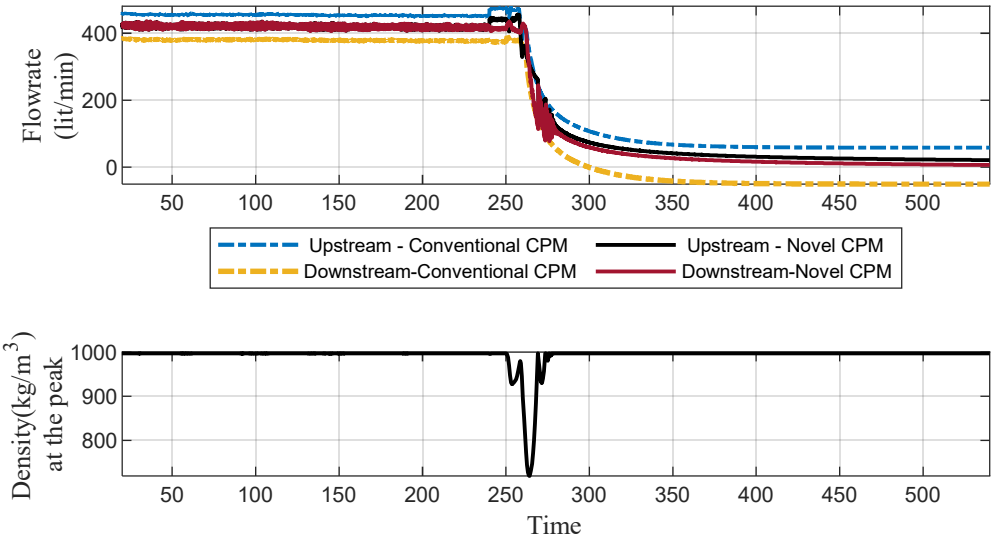

Figure 30- CASE NO. 13

(Top: pressures from PITs, Middle: flowrates of Novel CPM, Bottom: Modified flowrate of Conventional CPM)

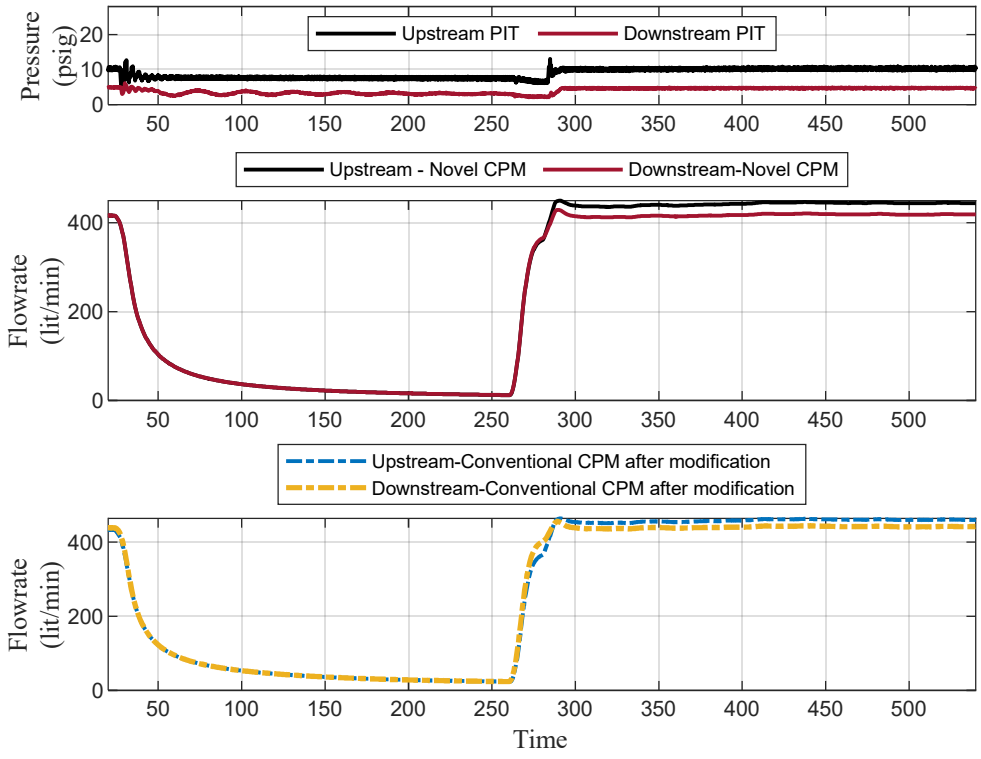

Figure 31- CASE NO.13

(Top: flowrates of Novel CPM and Conventional CPM without modification, Bottom: changes of the density at the peak)

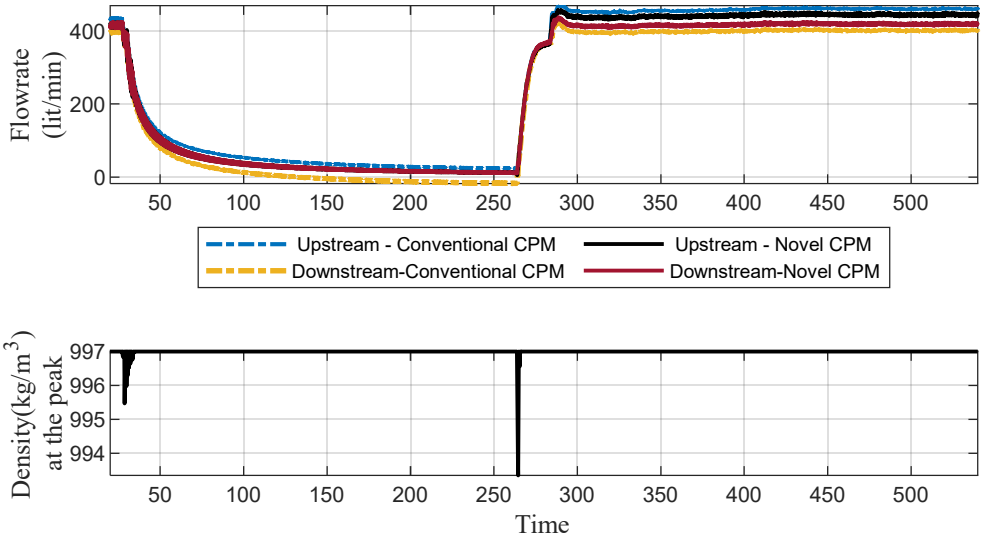

Figure 32- CASE NO. 14

(Top: pressures from PITs, Middle: flowrates of Novel CPM, Bottom: Modified flowrate of Conventional CPM)

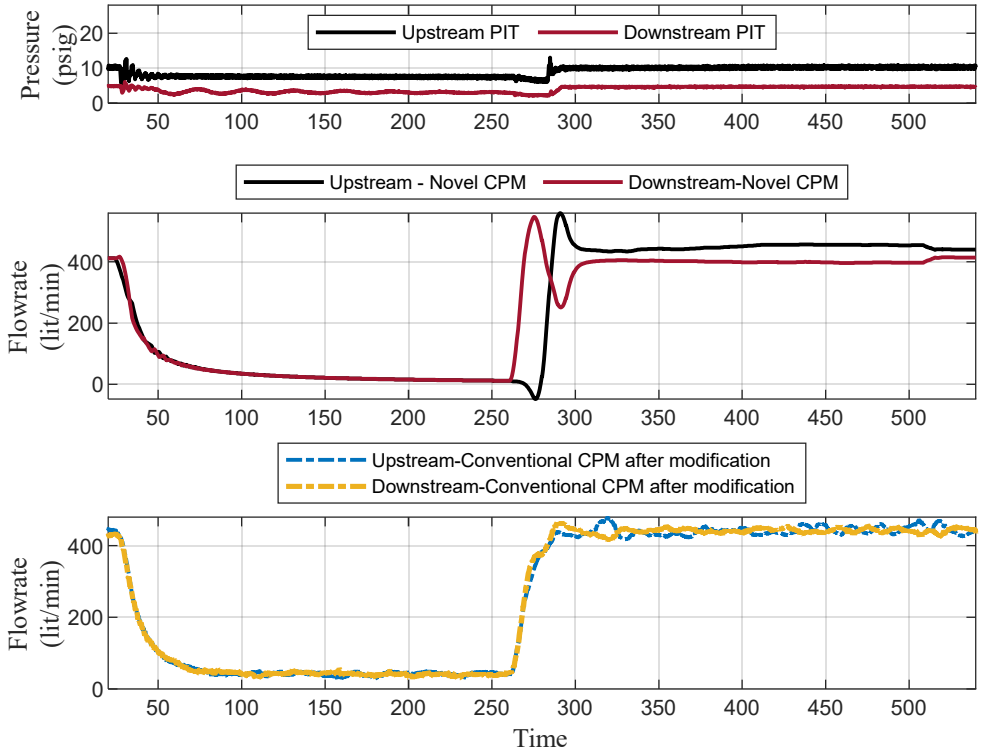

Figure 33- CASE NO. 14

(Top: flowrates of Novel CPM and Conventional CPM without modification, Bottom: changes of the density at the peak)

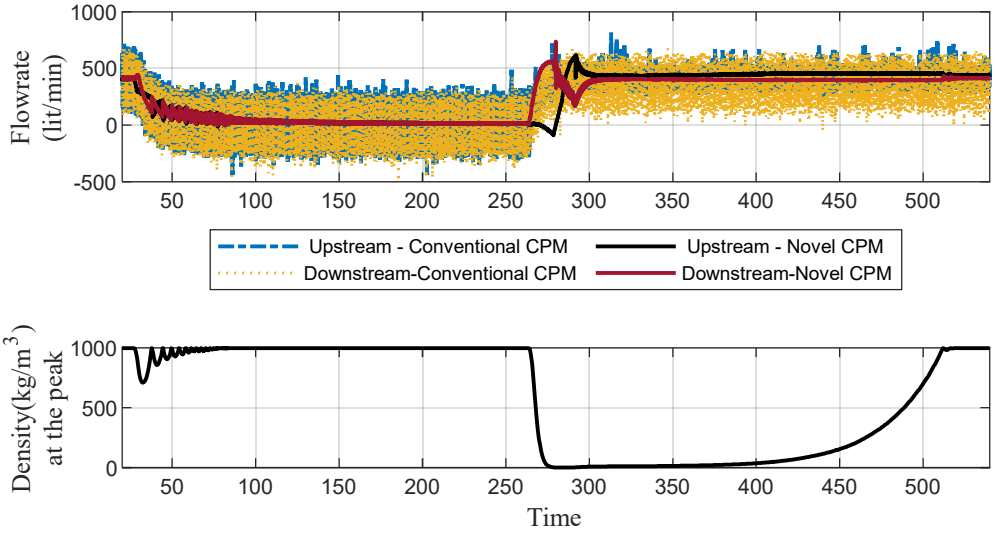

Figure 34- Left: flowrates of Novel and Conventional CPM without modification,
Right top: moving average of flowrates, Right bottom: Conventional CPM flowrates after resolving the imbalance.

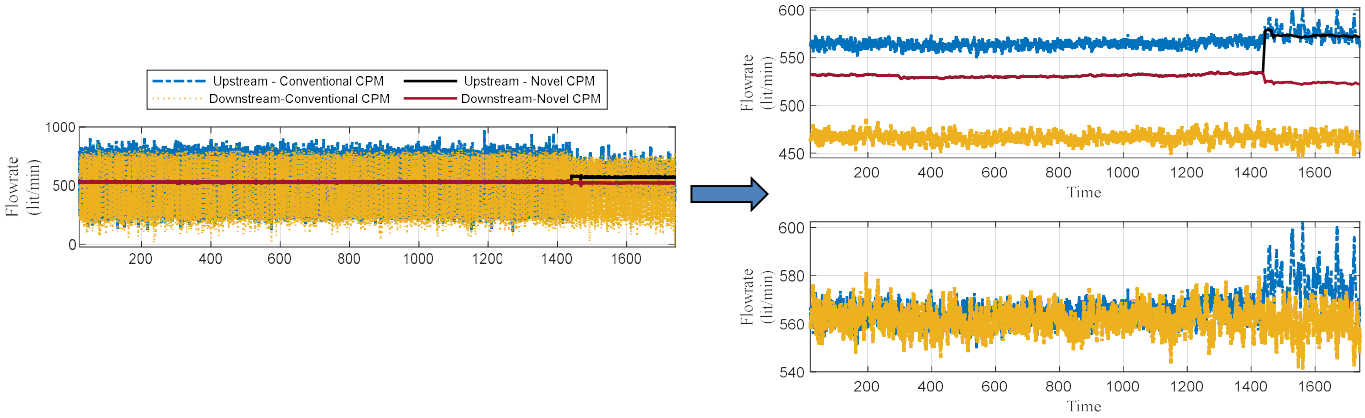

Figure 35- CASE NO.14 – Difference between Phases flowrates

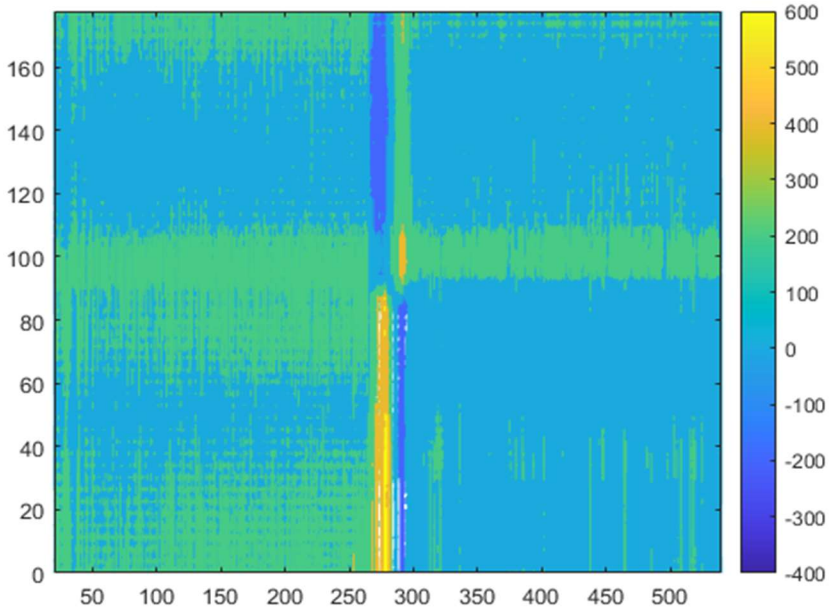

Figure 34-Artificial Constraints required in the Algorithm of the Conventional-Models-Based CPMs.